Limnol. Oceanogr., 55(5), 2010, 2085–2096

doi:10.4319/lo.2010.55.5.2085

Variability in the average sinking velocity of marine particles

Andrew M. P. McDonnell* and Ken O. Buesseler

Marine Chemistry and Geochemistry Department, Woods Hole Oceanographic Institution, Woods Hole, Massachusetts

Abstract

We used a new combination of sampling techniques involving in situ imaging of particles in the water column and the collection of particle flux in viscous polyacrylamide gels to estimate the average sinking velocities ($W_{i,\mathrm{avg}}$) of marine particles ranging from equivalent spherical diameters of 70 μm to 6 mm at several locations, depths, and times along the west Antarctica Peninsula to explore the variability of $W_{i,\mathrm{avg}}$. During the January 2009 deployments, $W_{i,\mathrm{avg}}$ ranged from about 10 to 150 m d^{-1}, with the fastest velocities at the large and small ends of the sizes considered. A repeat occupation of one station in Marguerite Bay in February 2009 gave $W_{i,\mathrm{avg}}$ size distributions that were quite different from those of the previous month, with rapidly sinking small particles and very slow $W_{i,\mathrm{avg}}$ for the large particle classes. These results demonstrate the importance of diatom aggregates and krill fecal pellets with regard to the ocean's biological pump in this region. The observed variability in space and time indicates that global relationships between particle concentrations and fluxes, or simple theoretical formulations of sinking velocity as a function of particle size (such as a single parameterization of the Stokes' Law), are unsuitable for yielding accurate estimates of particle flux from measurements of the particle size distribution. Combining measurements of $W_{i,\mathrm{avg}}$ with high-frequency sampling of the particle concentration size distribution would enable the estimation of particle fluxes at much higher temporal and spatial resolutions than is currently possible with conventional sediment trapping methods.

The sinking of biogenic particulate matter is the central component of the ocean's biological pump, by which carbon and other bio-active and particle-reactive elements are transported into the ocean's interior (Volk and Hoffert 1985). This process plays a major role in determining the distributions of many elements throughout the oceans and in controlling the air–sea balance of carbon dioxide (Broecker and Peng 1982; Fowler and Knauer 1986; Sarmiento and Gruber 2006). One of the dominant factors that sets the strength and efficiency of the biological pump is the velocity at which this particulate matter sinks from the euphotic zone to depth. Decades of studies have revealed that the sinking velocities of marine particles range over several orders of magnitude (Turner 2002), and no single formulation of the Stokes' Law seems to be able to account for this wide range in observed velocities (Stemmann et al. 2004, fig. 2).

The measurement and interpretation of the sinking velocities of natural marine particles has proved to be a difficult undertaking. Settling speeds have been measured in laboratory settling columns (Silver and Alldredge 1981; Gorsky et al. 1984; Hansen et al. 1996); however, the collection, handling, and storage of these fragile particles can easily change their physical characteristics and settling speeds. Others have directly observed sinking particles via carefully choreographed self-contained underwater breathing apparatus experiments in surface waters (Shanks and Trent 1980; Alldredge and Gotschalk 1988) or with in situ settling columns that use cameras to track the progress of particles as they sink through the field of view (Diercks and Asper 1997; Asper and Smith 2003). Time-series analysis of sediment traps at different depths has also been used to infer velocities from the time lag between flux events at different trap depths (Honjo 1996; Xue and Armstrong 2009). In addition, sophisticated sediment traps with indented rotating spheres and rotating sample cups allowed for the sorting of the flux into discrete groups as a function of sinking velocity (Peterson et al. 2005; Trull et al. 2008; Lee et al. 2009). These various methods and measurements have produced estimates of sinking velocities for marine particles that span a huge range of $\sim$ 5 to 2700 m d^{-1} but that commonly lie between tens to a few hundred of meters per day (Turner 2002; Armstrong et al. 2009). Results from settling columns, flux-timing experiments, and settling velocity traps are all fundamentally different measurements, and each type of sinking velocity must be interpreted and applied in very specific ways (Armstrong et al. 2009).

Recent advances in digital in situ imaging systems have made possible the rapid and high-resolution measurement of particle abundances and size distributions in the water column, as reviewed by Stemmann et al. (2004). These developments have intensified our need for a robust understanding of particle sinking velocities because the particle concentration (C_i, No. m^{-3} μm^{-1}) obtained from these instruments can be used to calculate the downward particle flux (F_i, No. m^{-2} d^{-1} μm^{-1}) if the average sinking velocities ($W_{i,\mathrm{avg}}$, m d^{-1}) for size class, i, are known, thus:

$$F_i = C_i \times W_{i,\mathrm{avg}} \quad (1)$$

Thus, knowledge of the average sinking velocities of marine particles and their variability with respect to location, depth, time, and particle size is essential for the utilization of in situ imaging systems as a tool with which to study the dynamics of the ocean's biological pump. Unfortunately, the methods described above for measuring sinking velocities are not usually appropriate for the oceanographic application of Eq. 1 because they tell us little about the

* Corresponding author: drewmcd@whoi.edu

actual relationship between the downward flux and the concentration of the highly heterogeneous collection of particles that exists in the water column at any given place or time.

To our knowledge, only one study (Asper 1987) has directly compared the flux size distribution (FSD = ΣF_i) with the concentration size distribution (CSD = ΣC_i), but this was done over 20 yr ago, when quantification of particle flux and concentration was done painstakingly with film cameras. A few recent imaging studies have analyzed the relationship between the CSD and the bulk particle flux, as collected in sediment traps (Walsh and Gardner 1992; Guidi et al. 2008; Iversen et al. 2010). For the first time, this technique has allowed for the high-resolution mapping of particle fluxes estimated from the CSD. However, standard sediment traps give only the total flux summed over all particle sizes, and therefore they cannot provide explicit information about the relationship between the CSD and the FSD. Instead, the above-described studies relied on the assumption that a single power law model based on Stokes' Law can adequately describe the sinking velocity as a function of particle size, implying that larger particles always sink faster than smaller ones. Additionally, the single relationship used by Guidi et al. (2008) was derived from a collection of loosely paired bulk flux and CSD data from several regions and depths throughout the ocean. Their approach, therefore, does not take into account any spatial or temporal variability that may arise in the relationship between flux and CSD as a result of changes in particle density, drag coefficients, source, type, geometry, composition, or other factors that may influence the sinking velocity of particles (Berelson 2002; De La Rocha et al. 2008; Ploug et al. 2008). In fact, Iversen et al. (2010) applied the relationship derived by Guidi et al. (2008) to measurements of the CSD at a study site off Cape Blanc, Mauritania, and found that it led to estimates of sinking fluxes that were a factor of 10 smaller than what was measured in sediment traps at the site. This indicates that there exists a wide range of relationships between particle fluxes and concentrations throughout the oceans, and a single parameterization of sinking velocity derived from a quasi-global relationship is not capable of accurately predicting fluxes from measurements of the CSD.

To improve the utility of in situ imaging systems in the study of the biological pump, oceanographers need a robust method with which to determine the average sinking velocity distribution (ASVD = $\Sigma W_{i,\mathrm{avg}}$) for all sizes of particles involved in this process. It is also necessary to make these measurements on temporal and spatial scales that sufficiently capture the inherent variability in the ASVD.

In this study, we overcome some of the limitations of bulk particle flux measurements from traps by employing the use of viscous polyacrylamide gel traps to collect the flux as individual particles during a short, 36-h deployment of a drifting array, thereby making it possible to quantify the FSD at multiple depths (Jackson et al. 2005). By dividing F_i by simultaneous measurements of C_i from an in situ imaging system at the drifter site, we calculated $W_{i,\mathrm{avg}}$ for each size class (Eq. 1). The results allow us to document the variability of the ASVD at different locations, depths, and times. This method for determining the average sinking velocities of marine particles is advantageous because it does not rely on theoretical assumptions about the variation of sinking velocity as a function of particle size and it negates the need to utilize empirical or hard-to-measure parameters in the calculation of sinking velocities from formulations such as Stokes' Law. Moreover, since $W_{i,\mathrm{avg}}$ is the average downward velocity of all the particles present in a given size class, it accounts for the neutrally and positively buoyant particles that have the potential to influence the CSD but not the downward flux (Asper et al. 1992; Azetsu-Scott and Passow 2004). In effect, the ASVD informs us about the actual relationship that exists between the particle concentration and the sinking flux.

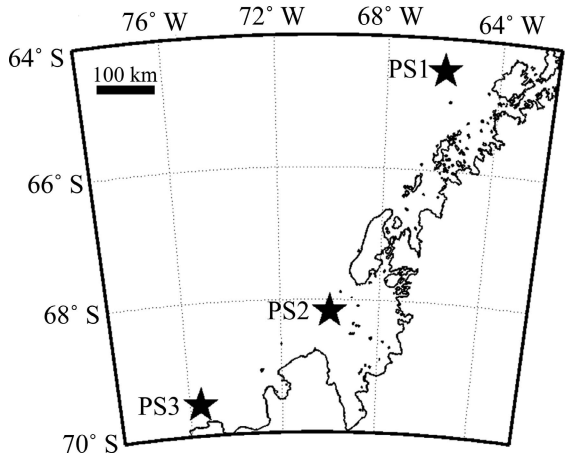

Fig. 1. Simultaneous measurements of particle flux and concentration were conducted at three process study (PS) stations on the continental shelf along the west Antarctic Peninsula from January through March 2009. PS1 and PS2 were each occupied twice during the season, allowing for temporal coverage.

Methods

Measurements of particle CSD and FSD were collected during a pair of cruises along the west Antarctica Peninsula (WAP) from January through March 2009. Our study was conducted in the region of the multi-decadal Palmer Long-Term Ecological Research (PAL) study (Ducklow et al. 2007). We focused our efforts at three process study stations (PS; Fig. 1). PS1 (64°29.3′S, 65°57.6′W) was located at the northern end of the study area at the site of the PAL moored time-series sediment trap. PS2 (68°10.5′S, 69°59.8′W) was located at the head of Marguerite Bay, while PS3 (69°31.9′S, 75°30.7′W) was located in the far south portion of the study area, about 20 km north of Charcot Island.

Measurement of the particle concentration size distribution—The concentrations of particles in the water column were measured with the Autonomous Video Plankton Recorder (VPR), manufactured by Seascan. The VPR is an underwater video microscope system that takes still images

Table 1. Particles were divided into one of 11 size bins according to their computed ESD. These bins are logarithmically spaced and defined by the ESD limits listed in this table.

ESD bin	Lower limit (μm)	Upper limit (μm)
1	45	73
2	73	120
3	120	195
4	195	320
5	320	520
6	520	850
7	850	1400
8	1400	2290
9	2290	3740
10	3740	6110
11	6110	10,000

of particles in an undisturbed parcel of water located between the camera housing and strobe illuminator as the instrument is lowered and raised through the water column on a nonconducting wire at approximately 30 m min^{-1}. A full description of the instrument can be found in Davis et al. (1996).

At a profiling velocity of 30 m min^{-1} and a sampling frequency of 12 Hz, overlapping image volumes are possible as a result of ship rolling, but based on successive image analysis, these events are rare. Nevertheless, we attempted to avoid overlapping images and double counting of particles by utilizing only every second image from the vertical profile. We conducted two vertical profiles at each location, and data were utilized from both the up-casts and the down-casts. The images were analyzed with a custom routine we wrote in MATLAB (The MathWorks) using the image analysis toolbox. Images were converted into gray scale, and a threshold was applied to detect regions of interest (ROIs) in the image, yielding a binary map of detected particles. These binary ROIs were then run through a dilation–erosion routine with a 3-pixel disk structuring element (González et al. 2004) to bridge small gaps between loosely associated particles held together by transparent exopolymeric particles (Passow et al. 2001). The number of pixels associated with each particle was used to calculate the projected particle area in square micrometers. Particles were binned into discrete size bins (Table 1) based on their equivalent spherical diameters (ESDs), where ESD is defined as the diameter of the sphere with the same projected area as the imaged particle. It is important to note that ESD is not a perfect description of particle size for particles that have shapes that deviate from that of a sphere. Errors may arise because of rotational asymmetries in particles and because of the fact that the VPR only views particles from a single direction.

We used zoom setting 'S2' on the VPR, which produces a field of view of 2.14 × 2.15 cm and a depth of field of 13.4 cm. The depth of field was calibrated using a transparent polycarbonate plate with many small holes drilled at regular intervals. This target was moved through the image volume at known intervals, and images were processed as usual with a gray-scale threshold. Each hole on the target that is within the image volume produces a round particle-like ROI in the captured images. In this manner, the number of ROIs detected was plotted as a function of target distance. The distances at which the slope of this curve reach a maximum and minimum were defined as the limits of the depth of field. In addition, the distance (in pixels) between the centroids of adjacent ROIs was divided by the known distance (in micrometers) between the holes in the polycarbonate target in order to calculate the ratio of pixels per millimeter in the image plane. We found that throughout the image volume, this ratio varied from 43 to 51 pixels mm^{-1}, with a larger ratio at the end of the depth of field closest to the camera. This variability introduces some errors into the determination of each particle's size, but this error is likely to be distributed in a Gaussian manner around the average value of 47 pixels mm^{-1}. Variation of the parameters used in the image analysis routines can also affect the results achieved. We explored a variety of different image-processing parameters for the VPR images via manual tuning and subsequent evaluation and verification of the processed images.

The particle CSD was calculated by dividing the number of particle counts for each size bin by the total imaged volume, where the total imaged volume is equal to the number of images analyzed in that 50-m depth range multiplied by the image volume of each VPR photograph. Under typical deployment configurations, the total imaged volume for each 50-m depth bin is approximately 150 liters. Each size-specific number concentration value, C_i, was then normalized by the width of the logarithmically spaced size bin that it occupied (Table 1), giving particle CSD in the following unit: No. m^{-3} μm^{-1}. The sizes of the depth intervals and particle size bins were chosen somewhat arbitrarily to balance the competing concerns of high resolution with respect to depth and particle size vs. the uncertainties that arise in the CSD from a small number of particle counts in increasingly higher resolution bins. Uncertainty in the observed CSDs was of particular concern for the largest particles in the size range sampled by the VPR because they are so rare that they needed to be grouped into increasingly larger size bins (hence, the logarithmic bin spacing of Table 1), and a large volume of water needed to be sampled (this was accomplished by using 50-m depth bins).

The CSDs used in this study were determined from VPR deployments conducted during the 36-h collection phase and within 1 km of the drifting polyacrylamide gel traps described below. This proximity is essential to this type of comparison study in order to ensure that measurements of the particle flux and concentration are representative of the same particle populations.

Measurement of the particle flux size distribution—Drifting sediment trap arrays were deployed to measure the sinking flux of particulate matter. The drifter was configured with traps at three depths, where the depths were spaced from about 25 m below the base of the euphotic zone down to 100 m above the bottom. Cylindrical traps with a collection area of 0.0113 m^2 and a height of 70 cm were outfitted with a polycarbonate jar

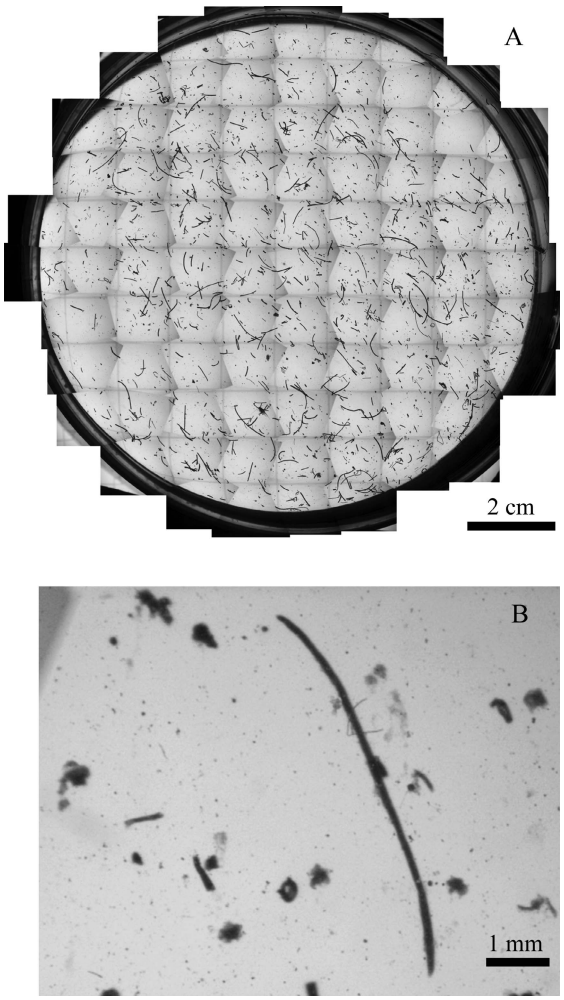

Fig. 2. Viscous polyacrylamide gels are placed in the base of drifting cylindrical sediment traps to collect intact sinking particles and preserve their individuality. These gels are systematically photographed with a microscope and analyzed in MATLAB, yielding the particle size distribution of the sinking flux. (A) An overall image of the gel created by merging 87 photographs. (B) Detail of the same gel samples, showing the range of particle sizes and types. Krill fecal strands and small diatom aggregates dominate the sinking flux. This gel was collected at PS1 on 05–06 March 2009 (a 35.5-h collection duration) at a depth of 150 m.

containing 200 mL of 16% polyacrylamide gel (Fig. 2), a method used in several previous studies (Lundsgaard 1995; Waite and Nodder 2001; Ebersbach and Trull 2008). The gel jar took up the entire area at the base of the trap cylinder. We followed the gel preparation protocol described in F. Ebersbach (unpubl.). Traps collected particles for 36 h, after which lids were closed, and the drifting array was retrieved within 36 h of the end of the collection period. Upon retrieval, the gel tubes were allowed to sit for 12 additional hours in order to ensure full penetration of the sinking particles into the viscous gel media.

The polyacrylamide gels were photographed with a with a Nikon SMZ-1500 stereomicroscope outfitted with a 1-megapixel digital camera in order to produce images for the analysis of particle size and abundance in the particle flux (Jackson et al. 2005). We used transmitted light, the widest zoom (0.75X objective), and a narrow aperture to maximize the depth of field and allow for the imaging of all the particles in the gel. A faint grid (1×1 cm) was printed on a transparency film and secured underneath the gel jar, facilitating the systematic photography of the gel over its entire area. This process yielded about 80 images that were subsequently merged together manually with the photomerge tool in Photoshop (Adobe Creative Suite 2). These large composite images measure about 50 megapixels and are capable of resolving particles over a large range of sizes ($\sim$ 50 μm to several centimeters in diameter; Fig. 2). The large composite image was cropped to remove the edges of the gel jars and then processed with Photoshop's edge detection and threshold algorithms. The result is a binary image that identifies the two-dimensional projected shape and area of each particle. Occasionally the large fecal pellets collected in the gels would overlap. To avoid counting two particles as a single larger one, these images were manually edited to separate overlapping particles while preserving the original particle size and shape. The processed binary images were then analyzed in MATLAB in the same manner as those from the VPR. This gives a particle FSD that is reported as the number of particles collected per unit area per time, and then normalized by the width of the logarithmically spaced size bins, and therefore is measured in the following units: No. m^{-2} d^{-1} μm^{-1}.

Flux collection biases could potentially affect our measurements of the particle FSD. In general, sediment traps are known to suffer from biases in the under- or overcollection of bulk fluxes. It is also possible that they may select or exclude certain particle sizes or types. Additionally, the flow of water across the trap opening could potentially break apart some of the most delicate aggregates if the fluid shear exceeds the particle's physical strength (Alldredge et al. 1990). The fact that we observed many large and intact diatom and detrital aggregates in the gels (*see* Results) indicates that there was no severe disaggregation taking place, but given the available data, we cannot rule out the possibility that this process was occurring to some extent. We deployed an acoustic current meter (Falmouth Scientific) at the bottom of the drifting array to measure the water velocities relative to the polyacrylamide gel traps. Relative water velocities were typically at or below 10–15 cm s^{-1}, placing the collection conditions within the range of velocities in which hydrodynamic flux-biasing concerns are thought to be minor for cylindrical traps with high aspect ratios (Gardner 2000). Moreover, the 'Clap' trap design used in this study did compare favorably to neutrally buoyant sediment traps with respect to flux and composition in studies conducted in the North Pacific (Lamborg et al. 2008). Unfortunately, the quantitative effects of these types of biases are notoriously difficult to ascertain and predict (Buesseler et al. 2007). Also, like all current sediment trap designs, the gel traps only measure the downward fluxes of particles, and any ascending particles (Azetsu-Scott and Passow 2004) that may be present in the water column would not be accounted for in the flux measurement.

Calculation of average sinking velocities—With measurements of the particle FSD and CSD we calculated the ASVD at each location and time at which there were simultaneous measurements of particle flux and concentration. This was done by dividing F_i by C_i (Eq. 1), giving $W_{i,\mathrm{avg}}$ in units of meters per day. Based on this methodology, if neutrally or positively buoyant particles are present in the water column, they would contribute velocities of 0 m d^{-1} to the average, as they would be detected with the VPR but not collected in the polyacrylamide gel traps.

Error analysis—The errors associated with each particle flux and concentration measurement are dependent on the number of particles detected in each case. Following counting statistics theory, the standard deviation associated with each measurement was computed as the square root of the number of particle counts. Thus, the greater the number of particle counts, the smaller the relative error. The error in $W_{i,\mathrm{avg}}$ was computed via propagation of error from the relative errors in the flux and concentration data using the formulation appropriate for the division of two variables,

$$\frac{\sigma_{W_{i,\mathrm{avg}}}}{W_{i,\mathrm{avg}}} = \sqrt{\left(\frac{\sigma_{F_i}}{F_i}\right)^2 + \left(\frac{\sigma_{C_i}}{C_i}\right)^2 - 2\frac{\sigma_{F_i}\sigma_{C_i}}{F_i C_i}\rho_{F,C}} \qquad (2)$$

where $\rho_{F,C}$ is the Pearson's correlation coefficient and σ is the standard deviation of each respective variable. Using all of the flux and concentration data pairs in this study, we determined a $\rho_{F,C}$ of 0.74.

Results

The high resolution of the merged gel images allowed for the accurate determination of particle flux from ~ 44 μm to 2300 μm. Smaller particles were unable to be reliably resolved, and particles larger than 2300 μm were so rarely collected in the polyacrylamide gel traps that it was difficult to quantify their exact flux. The measured particle fluxes in this size range varied from to 10^{-1} particles m^{-2} d^{-1} μm^{-1} for the largest particles to 7×10^4 particles m^{-2} d^{-1} μm^{-1} for the smallest size class (Figs. 3–5). A close visual inspection of the gel images reveals that most of the particles could be separated into two distinct particle types: small particles that are nearly spherical and long cylindrical fecal pellets (Fig. 2). The small particles include diatom aggregates, detritus, and protozoans and their minipellets (González 1992), while the large cylindrical fecal pellets are primarily from the Antarctic krill species *Euphausia superba* (D. Steinberg pers. comm.). The fact that we observed marine snow aggregates still intact in the gel indicates that the gel trap is quite effective at preserving the structure of even the most fragile particles.

Particle concentrations ranged from 10^{-2} to 10^3 particles m^{-3} μm^{-1} (Figs. 3–5) and followed patterns, with respect to ESD, similar to those widely observed for collections of natural particles in the ocean (Jackson et al. 1997; Guidi et al. 2008). The detectable size range from the VPR was slightly more restricted than that of the polyacrylamide gel traps and reliably ranged from 73 to 1400 μm. Particles larger than this were either not present or far too rare to quantify based on the volume of water imaged with the VPR. Additionally, on the zoom setting used in this study, the VPR has an image area of 2.14 × 2.15 cm, so particles that approach this size are unlikely to be fully imaged and therefore were omitted from the image analysis routine. As the large particles were the most rarely encountered, their concentrations are subject to the largest errors. The digital resolution of the VPR theoretically allows for the detection of particles as small as 25 μm, but this is approaching the size of an individual pixel and therefore is difficult to distinguish from image noise. There is also the potential for certain particles to be undersampled by the VPR, particularly at the small end of the size spectrum (Jackson et al. 1997). For this reason, we only report concentration data for particles with an ESD larger than 73 μm.

Average sinking velocities—During the January deployments at the three process stations, $W_{i,\mathrm{avg}}$ ranged from ~ 25 to 150 m d^{-1}, depending on the size class and location (Fig. 3C,F,I). The general pattern of the ASVD during January was similar among all three sites. The slowest velocities of ~ 25 m d^{-1} were found for particles with ESDs of about 120 to 320 μm. Particles with ESDs smaller than 120 μm and larger than about 320 μm sank more quickly than did those in the middle size classes. $W_{i,\mathrm{avg}}$ increased with increasing ESD, from ~ 320 μm up to 1400 μm for these three stations. Particles larger than 1400 μm were rare, and, as a result, it was difficult to accurately determine their fluxes and concentrations. When a few of the largest particles were observed (Fig. 3, open bars), the calculated $W_{i,\mathrm{avg}}$ generally showed elevated sinking velocities relative to other size classes at all three process stations in January, but the errors due to low particle counts prevent us from drawing firm conclusions about $W_{i,\mathrm{avg}}$ for the largest size classes.

The ASVD was also calculated at three different depths at each site. Figure 4 shows the flux, concentration, and calculated ASVD at 50, 150, and 250 m from the January 2009 deployment at PS1. There was some variability in $W_{i,\mathrm{avg}}$ with respect to depth, especially at the larger size classes (Fig. 4C,F,I). In particular, $W_{i,\mathrm{avg}}$ was significantly faster at 250 m, when compared to 150-m depth, for all size classes larger than 120 μm. At 50 m, the VPR showed low particle concentrations (Fig. 4B), which led to large errors in $W_{i,\mathrm{avg}}$ and greater variability with respect to ESD. At the deeper trap depths, particle concentrations were higher, and the errors associated with a small number of particle counts were less pronounced.

The ASVD did not always follow the same pattern of high velocities for the smallest and largest particles, as was observed at the three process stations in January. A repeat occupation of PS2 in late February yielded significantly different results (Fig. 5). In February, the smallest particle size bin had the fasted calculated $W_{i,\mathrm{avg}}$, 295 m d^{-1}, and the ASVD declined sharply as a function of ESD until the largest size class of 850–1400 μm, which had a $W_{i,\mathrm{avg}}$ of only 9 m d^{-1}. As discussed above, the ASVD observed in January at PS2 had high velocities for the largest particles and a high $W_{i,\mathrm{avg}}$ of 145 m d^{-1} for the smallest size class,

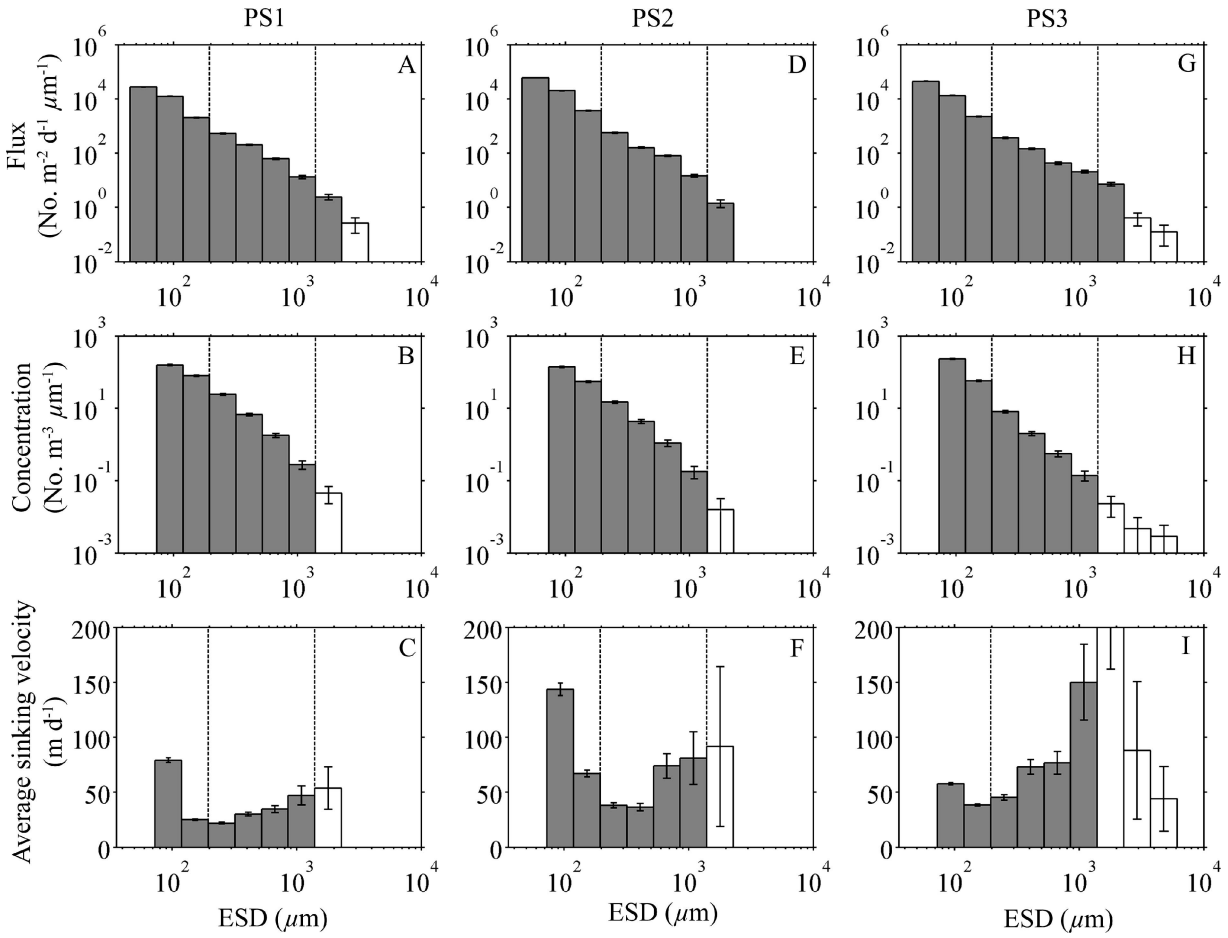

Fig. 3. Particle size distributions for three locations along the WAP illustrate the relationship between the (A, D, G) particle flux, (B, E, H) concentration, and (C, F, I) average sinking velocity. The calculated $W_{i,\mathrm{avg}}$ values range from ~ 20 m d^{-1} to ~ 150 m d^{-1}, with the highest velocities for the particles with the smallest and largest ESD collected in the traps. Intermediate-sized particles had the lowest velocities. Error bars display the standard deviations for each size bin. Open bars indicate that fewer than six particles were counted in that size bin, and therefore the associated errors are high and difficult to quantify, but we include these data for the additional information they may provide. Two vertical grid lines are used to aid the eye in the alignment of the different size classes. Flux data is from the 150-m trap at PS1 and PS3 and from the 200-m trap at PS2. CSD are averages from the 50 m of the water column immediately above the trap.

with particles in the middle of the size range having the slowest calculated average sinking velocities. Figure 5A and E show portions of the gels from PS2 during both the January and February occupations. In January, there was an abundance of large krill fecal pellets and few small particles collected in the polyacrylamide gel traps. Approximately 1 month later at the same location, large krill fecal pellets were not present in the gel traps, and there was an increase in the flux of the smaller aggregates and minipellets. The resulting ASVD values from these two occupations are markedly different.

Discussion

The fact that the highest sinking velocities were found in the largest and smallest size classes was a surprising result, especially given that most models of sinking velocity (e.g., Stokes' Law) predict increasing settling speeds as particle size increases. Closer inspection of the material collected in the polyacrylamide gel traps reveals that the majority of particles comprised two dominant particle sizes. Many individual diatoms and radiolarians were present with ESDs in the 70–120-μm size range. With their dense frustules and skeletons, these small particles were likely sinking quickly and therefore would have had high abundances in the gels relative to their measured concentrations in the water column. On the large end of the FSD, fecal strands from the Antarctic krill species *E. superba* dominated the flux and led to high $W_{i,\mathrm{avg}}$ in these size classes. Thus, it is likely that these two distinct particle groups sink very rapidly and therefore lead to high $W_{i,\mathrm{avg}}$ in their respective size bins. Previous direct measurements of the sinking velocities of Euphausiid fecal pellets range from 16 to 862 m d^{-1}, while marine snow was observed to have a more restricted upper limit, with sinking velocities of 16–368 m d^{-1} (Turner 2002). Fecal pellets generated by *E. superba* specimens from our January 2009 cruise had velocities of 200 m d^{-1}, as determined by laboratory settling column measurements (D. Steinberg pers. comm.). Our calculated $W_{i,\mathrm{avg}}$ values are consistent with these

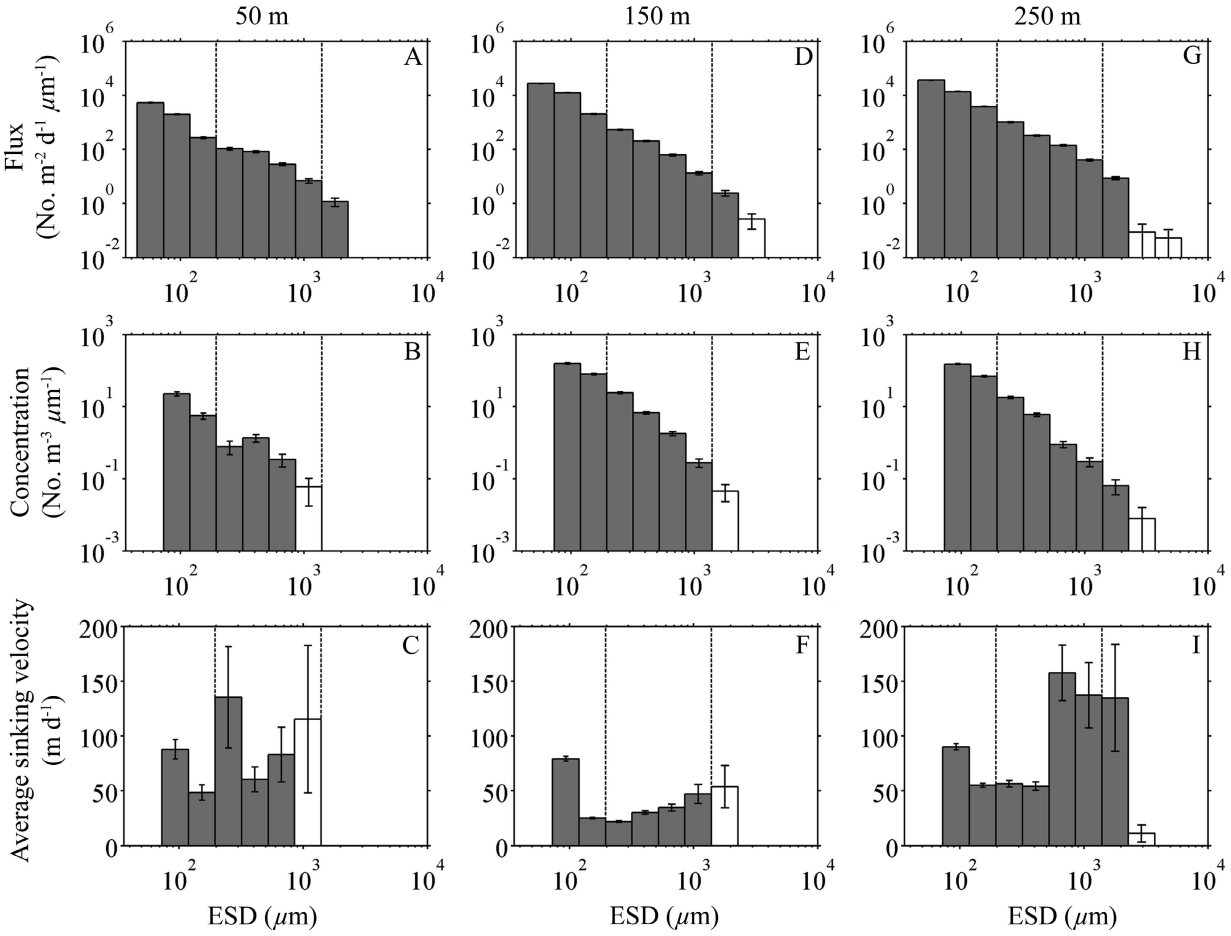

Fig. 4. Particle size distributions during the January 2009 occupation of PS1 illustrate the relationship between the (A, D, G) particle flux, (B, E, H) concentration, and (C, F, I) average sinking velocity at (A–C) 50 m, (D–F) 150 m, and (G–I) 250 m beneath the surface. Open bars indicate that less than six particles were counted in that size bin in either the flux or concentration. Two vertical grid lines are included to aid the eye in the alignment of the different size classes.

measurements. In addition, since $W_{i,\mathrm{avg}}$ is the average sinking velocity of all particles in the water column of a given size, we expect these values to be in the middle of the range of sinking velocities measured via direct methods, and this is in fact what we observed.

The subtle variations that exist between the three locations presented in Fig. 3 can be explained by real changes in the actual sinking velocities of individual particles, differences in the assemblages of particles present, or a combination of those two factors. Real changes in the sinking velocities of particles are possible and could occur for a variety of reasons. For example, the excess densities of particles could be different as a result of diet changes in the krill populations (Bienfang 1980). Changes in the fractal nature of aggregates could change their excess densities or drag coefficients (Stemmann et al. 2004). Another factor that could alter $W_{i,\mathrm{avg}}$ is differences in the types of particles present for a given size class, or even a shift in their relative abundances. In the case of PS3, the gel trap at 150 m contained many large aggregates made up of long fecal pellets joined to diatom aggregates. These joint fecal pellet–diatom aggregates were unique to this station and could be the reason why higher sinking velocities of 150 m d^{-1} were observed at this location for these large size classes.

The striking change in the ASVD between the two occupations of PS2 in Marguerite Bay (Fig. 5) illustrates how a seasonal succession in community structure can strongly affect the relationship between the flux and concentration of particles in the water column. Previous studies assumed this variability was insignificant and that a single parameterization relating bulk fluxes to CSD measurements was capable of accurately estimating particle flux from measurements of CSD (Guidi et al. 2008). However, our results demonstrate that this approach could introduce large errors if this variability is not properly accounted for.

Interpreting the variability in the ASVD—We explored how changes in the relative abundances of different particle types with characteristically different sinking velocities can affect the observed ASVD. This was accomplished by constructing a simple model of particle sinking velocities based on Stokes' Law. Noticing that the

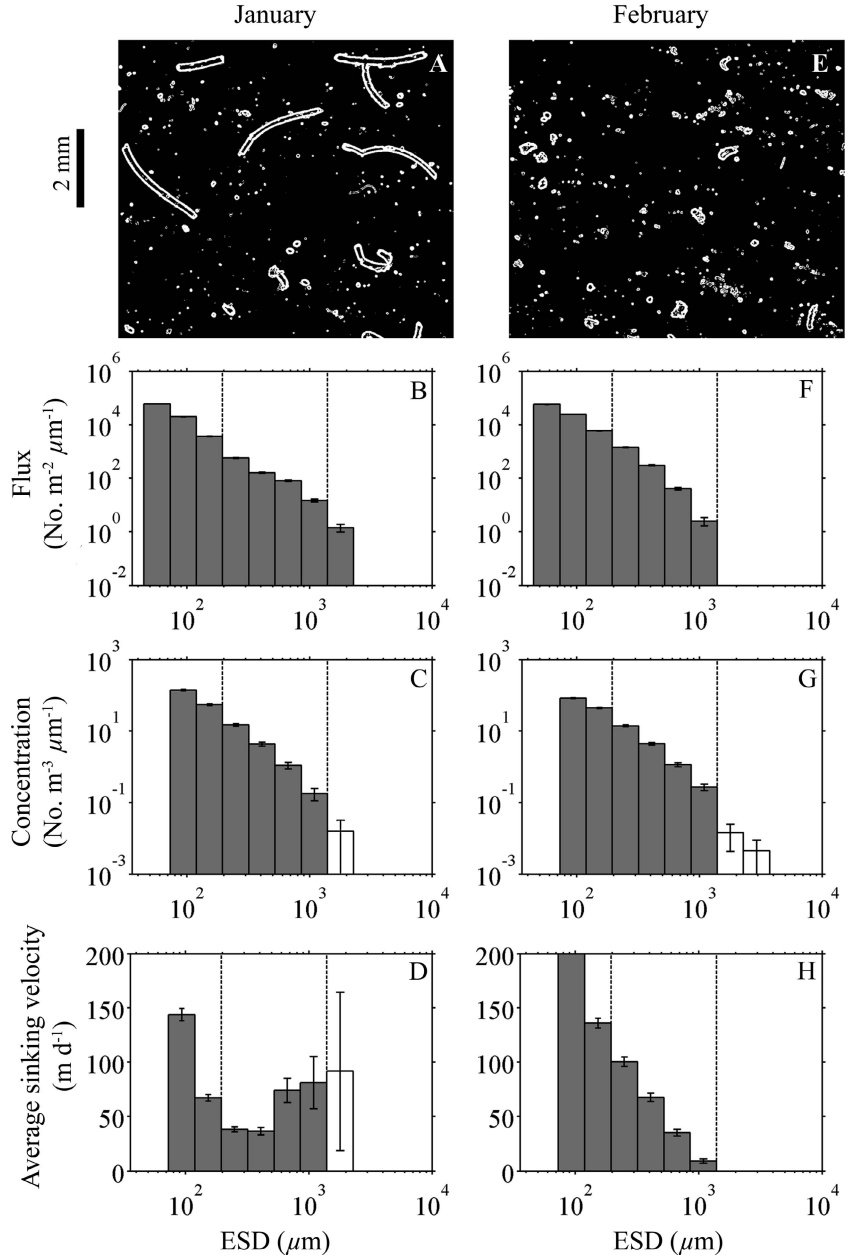

Fig. 5. (A) During the first occupation of the PS2 in January, the flux collected in the polyacrylamide gel traps consisted mostly of small spherical particles and large krill fecal strands. (B) In late February, the flux consisted primarily of small aggregates, while the large fecal strands were absent. (B, F) These conditions caused changes in the FSD. (C, G) In addition, the CSD was significantly different between the 2 months. (D, H) These variations led to substantially different ASVD. Note that the $W_{i,\mathrm{avg}}$ of the small size class for panel F is off scale, at 250 m d^{-1}. Two vertical grid lines are included to aid the eye in the alignment of the different size classes.

flux of particles collected in the gel traps consisted primarily of two distinctive particle types, small spherical particles and large cylindrical fecal pellets, we utilized the appropriate permutations of Stokes' Law to describe the sinking velocities of these two particle groups as a function of particle size.

For the spherical particles typical of the small size classes, we used the standard form of Stokes' Law given by

$$W_{\mathrm{sphere}} = \frac{2(\rho_p - \rho_f) r^2 g}{9\mu} \quad (3)$$

where W_{sphere} is the sinking velocity of a solid sphere, r is the particle radius, g is the acceleration of gravity, ρ_p and ρ_f are the densities of the particle and fluid, respectively, and μ is the dynamic viscosity of the seawater. We utilized a dynamic viscosity typical of WAP waters

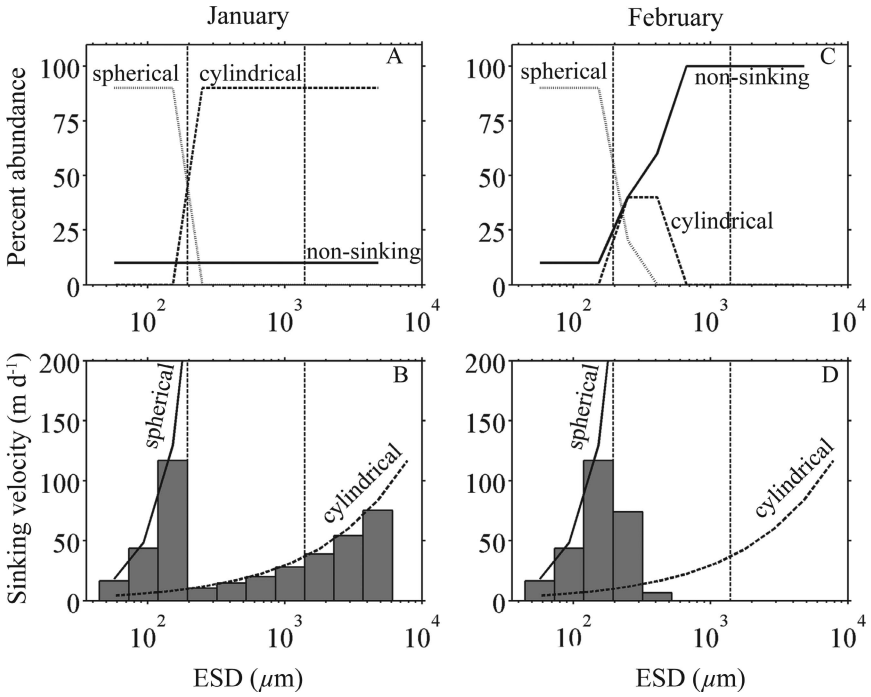

Fig. 6. Here we present a simple model to aid in the interpretation of the large variability in the ASVD observed between the two occupations of PS2. The model features three types of particles (small spherical, large cylindrical, and non-sinking particles), each with their own characteristic sinking velocities. (A, C) The model inputs of relative particle abundances for the three functional groups of particles as a function of ESD. (B, D) The modified Stokes' Law sinking velocities for the two sinking particle types (solid and dashed curves) and the ASVD (bars) that would be expected based on the different particle abundance scenarios in panels A and C. (A, B) Representative of the relative particle abundances present at PS2 in January, while (C, D) are representative of conditions during the February occupation of PS2. These results illustrate how the presence or absence of certain particle types in the water column can lead to large variability in the ASVD and how ASVD values do not always follow a pattern of increasing sinking velocity as a function of ESD, as predicted by single particle type formulations of Stokes' Law. Two vertical grid lines are included to aid the eye in the alignment of the different size classes.

(1.88×10^{-3} Pa s) and a particle density, ρ_p, of 1.25 g cm^{-3} to be representative of the diatomaceous matter of the particles at the smaller end of the size spectrum (Sicko-Goad et al. 1984). This parameterization is plotted as the solid curves in Fig. 6B and D.

The second particle type we considered was cylindrical fecal pellets. We use the semiempirical equation reported by Komar (1980) for cylindrical particles at low Reynolds numbers, thus:

$$W_{\text{cylinder}} = \frac{0.079(\rho_p - \rho_f)\mathrm{L}^2 g}{\mu}\left(\frac{\mathrm{L}}{\mathrm{D}}\right)^{-1.664} \quad (4)$$

We determined an average fecal pellet diameter (D), of 120 μm from the gel images. The fecal pellet length (L) was then calculated by dividing the projected particle area for each ESD size bin by D. We used a particle density of 1.174 g cm^{-3}, as this was carefully determined for krill fecal pellets produced under a natural diet of diatoms (Bienfang 1980). The dashed curves in Fig. 6B and D show the sinking velocities of krill fecal pellets as a function of ESD. As expected, the cylindrical particles have slower velocities than their spherical counterparts as a result of the higher drag forces acting upon them. In addition, the sinking velocity of the cylindrical fecal pellets increases more slowly, as a function of ESD, than does that of the spherical particles.

In order to account for the dominance of the spherical type particles in the smaller size classes and the cylindrical fecal pellets in the larger size classes, we varied the relative abundances of the two particle types across the observable size spectrum in a manner that was representative of the particle populations observed in both the January and February occupations of PS2. These inputs of relative particle abundance are described in graphical form in Fig. 6A and C. In addition to the two categories of sinking particles, we included a third neutrally buoyant particle type (sinking velocity equal to zero at all sizes), the relative abundance of which was estimated by analyzing the differences between the FSD and the CSD. In the case in which there was a high concentration of large particles present in the water column but very few found in the gels, we assumed that there was a large proportion of non-sinking particles. The average sinking velocity was then

computed for each size class as the abundance-weighted average of the spherical, cylindrical, and non-sinking particle velocities and plotted as bar graphs in Fig. 6B and D. It is important to note that we use this simple model solely to aid in the interpretation of our experimentally determined ASVD in this particular region. It is formulated in a way that is specific to the observations of particle types that we made along the WAP in 2009, and, therefore, we don't recommend its wide or general application as a predictive model of particle flux.

In the model run parameterized to represent the relative abundances present in January, the ASVD came to a local maximum of 120 m d^{-1} at an ESD of 150 μm, and it decreased to slower velocities for particles with an ESD of between 250 and 1000 μm (Fig. 6A,B). Between 400 μm and 9 mm, $W_{i,\mathrm{avg}}$ increased as a result of the increasing velocities of the cylindrical fecal pellets as a function of particle size (Fig. 6B, dotted curve). A comparison of the modeled ASVD in Fig. 6B to the observed ASVD in Fig. 5D reveals similarities in both the magnitude of the velocities and their dependencies on particle size.

Can this simple model be used to explain the major change we observed in the ASVD at PS2 between January and February? We addressed this question by conducting a second model run, this time without the large cylindrical fecal pellets (Fig. 6C), similar to the conditions observed in February at PS2. As we expect, in the absence of cylindrical fecal pellets, the modeled ASVD drops quickly to very low velocities after peaking at an ESD of 150 μm (Fig. 6D), just as we observed during the February occupation of PS2 (Fig. 5H). It is worth noting that without the inclusion of a third non-sinking particle category, the modeled ASVD would continue to increase as a function of increasing size, in accordance with Stokes' Law. The observation that the ASVD dropped to almost zero at the larger size classes in the case of February's occupation of PS2 confirms the presence of significant quantities of very slow sinking or neutrally buoyant particles of those large sizes in the water column.

The results from this simple model indicate that the relative abundances of different particle types coupled with their characteristic sinking velocities can affect the ASVD in a manner that cannot be predicted from a single formulation of Stokes' Law. It is likely that the majority of the variations in the ASVD that we observed in this study were primarily driven by changes in the relative abundances of different types of sinking particles.

These ASVD results are important because several studies have attempted to estimate particle flux from the particle CSD (Guidi et al. 2007, 2008; Iversen et al. 2010). The framework for these flux estimates is almost always some modeled formulation of Stokes' Law, in which the sinking velocity is a function of the particle size, with the largest particles sinking fastest. Our observations of $W_{i,\mathrm{avg}}$ from the WAP demonstrate that for the heterogeneous collections of particles found in the water column, the velocities of these particles did not follow the pattern indicated by a single formulation of Stokes' Law. While Stokes' Law is clearly still valid for individual solid spherical particles at low Reynolds numbers, it is likely that variations in the excess density of particles and their drag coefficients result in ASVD values that are not easily predictable from measurements of ESD alone. This means that it is important to determine the ASVD through direct measurements, such as those presented in this article, in order to accurately estimate particle fluxes from the CSD. In addition, our results show that one general ASVD relationship is not applicable across all regional spatial scales and seasonal time scales in the ocean and that these paired measurements of flux and concentration need to be made on scales that appropriately capture the variability of the ASVD.

Another way to approach this question would be to sort particles by type rather than by arbitrary size classes. In the case of the WAP, particles could be classified into several categories, such as those mentioned above. This would allow us to use Eq. 1 to calculate the average sinking velocity for each particle type or even an ASVD for each particle type. Because we might expect particles of the same type to have similar sinking velocities, it is possible that classifying particles by type would remove some of the observed variability in ASVD that arises as a result of the presence, absence, or variable abundances of these different particle types, with their characteristic sinking velocities at various depths, locations, or times. This could potentially increase the range of spatial and temporal scales over which one determination of the ASVD is applicable, making it more useful in calculating particle fluxes from measurements of particle concentration. We are currently developing methods to automatically sort and identify particles in images from the VPR and the polyacrylamide gels in order to explore the utility of particle classification in the determination of average sinking velocities.

Multiplication of the CSD by the ASVD (Eq. 1) determined here could yield high-resolution estimates of the FSD. However, in order to convert this number flux into a biogeochemical flux, we would need to know the particle volume flux and carbon content of particles as a function of ESD. Volume flux can be calculated either by assuming all particles are spherical or by using a more sophisticated method that takes into account the shape of the two-dimensional projection of each particle. Converting the volume flux to a carbon flux requires knowledge of carbon content per unit volume of particle. Unfortunately, this parameter is poorly constrained and difficult to determine. Guidi et al. (2008) addressed the problem by fitting a power law relationship for a combined function of particle mass concentration and sinking velocity to bulk fluxes measured in sediment traps. Ebersbach and Trull (2008) relied on literature values of carbon density per particle volume for a few different particle types. Another way to do this would be to deploy in situ pumps with a few different mesh sizes. This would give a carbon concentration per unit volume of seawater as a function of nominal particle size. Comparison of these concentrations with the measured CSD would allow for an estimate of the carbon density of the particles. All of these methods carry with them significant uncertainties, and more work is needed to improve our understanding of organic carbon content per particle volume before in situ imaging of particles becomes

a valuable tool in estimating sinking carbon fluxes at high resolutions. Similarly, if the volume content of other interesting elements is able to be determined, it would be possible to use in situ imaging systems for the estimation of other elemental fluxes, such as nitrogen, particulate inorganic carbon, biogenic silica, etc.

The approach presented here represents a new way to quantify the ASVD of marine particulate matter. The results of this article highlight the fact that the ASVD is variable in space and time and depends on the relative abundances of particles as well as their respective sinking velocities. This variability implies that global relationships between particle concentrations and fluxes or simple theoretical formulations of sinking velocity as a function of particle size, such as a single parameterization of Stokes' Law, are unsuitable for yielding accurate estimates of particle flux from measurements of particle concentration. Instead, the ASVD should be determined frequently in order to best constrain the relationship between particle stocks in the water column and the sinking flux of particulate matter. This approach will aid in the elucidation of the mechanisms that control the flux of particulate matter into the ocean's interior and will be useful in the validation and testing of models of particle flux.

Acknowledgments

We thank the principal investigators of the Palmer Long-Term Ecological Research Program (PAL) and the Food For Benthos on the Antarctic Continental Shelf Project (FOODBANCS) for accommodating our science on their respective cruises to the west Antarctic Peninsula in 2009. The captain, crew, and Raytheon Polar Services Company staff aboard the Antarctic Research and Supply Vessel *Laurence M. Gould* and onshore did an excellent job helping us achieve our sampling objectives in this challenging work environment. We are very grateful to Tom Trull, who first suggested this approach. Scott Gallager, Mick Follows, Phoebe Lam, Phil Boyd, Debbie Steinberg, Dave Siegel, Dave Glover, and Stephanie Owens provided constructive comments and suggestions. James Valdes made possible much of the underwater instrumentation associated with the drifting sediment trap array. Seascan provided valuable technical support for the Video Plankton Recorder. We thank Adrian Burd, Thomas Kiørboe, and an anonymous reviewer for their comments, which greatly improved this manuscript during the review process. Funding was provided by the Woods Hole Oceanographic Institution (WHOI) Rinehart Access to the Sea Program, the WHOI Coastal Oceans Institute, WHOI Academic Programs Office, and the National Science Foundation (NSF) Office of Polar Programs for support of PAL, FOODBANCS, and west Antarctic Peninsula Flux projects. A grant from NSF Carbon and Water Program supported the development of these methods.

References

Alldredge, A. L., and C. Gotschalk. 1988. In situ settling behavior of marine snow. Limnol. Oceanogr. **33:** 339–351, doi:10.4319/lo.1988.33.3.0339

———, T. C. Granata, C. C. Gotschalk, and T. D. Dickey. 1990. The physical strength of marine snow and its implications for particle disaggregation in the ocean. Limnol. Oceanogr. **35:** 1415–1428, doi:10.4319/lo.1990.35.7.1415

Armstrong, R. A., M. L. Peterson, C. Lee, and S. G. Wakeham. 2009. Settling velocity spectra and the ballast ratio hypothesis. Deep-Sea Res. II **56:** 1470–1478, doi:10.1016/j.dsr2.2008.11.032

Asper, V. L. 1987. Measuring the flux and sinking speed of marine snow aggregates. Deep-Sea Res. **34:** 1–17.

———, S. Honjo, and T. H. Orst. 1992. Distribution of transport of marine snow aggregates in the Panama Basin. Deep-Sea Res. **39:** 939–952.

———, and W. O. Smith. 2003. Abundance, distribution and sinking rates of aggregates in the Ross Sea, Antarctica. Deep-Sea Res. I **50:** 131–150, doi:10.1016/S0967-0637(02)00146-2

Azetsu-Scott, K., and U. Passow. 2004. Ascending marine particles: Significance of transparent exopolymer particles (TEP) in the upper ocean. Limnol. Oceanogr. **49:** 741–748, doi:10.4319/lo.2004.49.3.0741

Berelson, W. M. 2002. Particle settling rates increase with depth in the ocean. Deep-Sea Res. II **49:** 237–251, doi:10.1016/S0967-0645(01)00102-3

Bienfang, P. K. 1980. Herbivore diet affects fecal pellet settling. Can. J. Fish. Aquat. Sci. **37:** 1352–1357, doi:10.1139/f80-173

Broecker, W., and T. Peng. 1982. Tracers in the sea. Lamont-Doherty Geological Observatory Eldigio Press.

Buesseler, K. O., and others. 2007. An assessment of the use of sediment traps for estimating upper ocean particle fluxes. J. Mar. Res. **65:** 345–416.

Davis, C. S., S. M. Gallager, M. Marra, and W. K. Stewart. 1996. Rapid visualization of plankton abundance and taxonomic composition using the Video Plankton Recorder. Deep Sea-Res. II **43:** 1947–1970, doi:10.1016/S0967-0645(96)00051-3

De La Rocha, C. L., N. Nowald, and U. Passow. 2008. Interactions between diatom aggregates, minerals, particulate organic carbon, and dissolved organic matter: Further implications for the ballast hypothesis. Glob. Biogeochem. Cycles **22:** GB4005, doi:10.1029/2007GB003156

Diercks, A. R., and V. L. Asper. 1997. In situ settling speeds of marine snow aggregates below the mixed layer: Black Sea and Gulf of Mexico. Deep-Sea Res. I **44:** 385–398, doi:10.1016/S0967-0637(96)00104-5

Ducklow, H., and others. 2007. Marine pelagic ecosystems: The West Antarctic Peninsula. Philos. Trans. R. Soc. B **362:** 67–94, doi:10.1098/rstb.2006.1955

Ebersbach, F., and T. Trull. 2008. Sinking particle properties from polyacrylamide gels during the KErguelen Ocean and Plateau compared Study (KEOPS): Zooplankton control of carbon export in an area of persistent natural iron inputs in the Southern Ocean. Limnol. Oceanogr. **53:** 212–224.

Fowler, S., and G. Knauer. 1986. Role of large particles in the transport of elements and organic compounds through the oceanic water column. Prog. Oceanogr. **16:** 147–194, doi:10.1016/0079-6611(86)90032-7

Gardner, W. D. 2000. Sediment trap technology and surface sampling in surface waters, p. 240–281. *In* R. B. Hanson, H. W. Ducklow, and J. G. Field [eds.], The changing ocean carbon cycle, a midterm synthesis of the Joint Global Ocean Flux Study. Cambridge Univ. Press.

González, H. E. 1992. Distribution of minipellets around the Antarctic peninsula. Implications for protistan feeding behaviour. Mar. Ecol. Prog. Ser. **90:** 223–236, doi:10.3354/meps090223

González, R. C., R. E. Woods, and S. L. Eddins. 2004. Digital image processing using MATLAB. Pearson Prentice Hall.

Gorsky, G., N. S. Fisher, and S. W. Fowler. 1984. Biogenic debris from the pelagic tunicate, *Oikopleura dioica*, and its role in the vertical transport of a transuranium element. Estuar. Coast. Shelf Sci. **18:** 13–23, doi:10.1016/0272-7714(84)90003-9

Guidi, L., G. A. Jackson, L. Stemmann, J. C. Miquel, M. Picheral, and G. Gorsky. 2008. Relationship between particle size distribution and flux in the mesopelagic zone. Deep-Sea Res. I **55:** 1364–1374, doi:10.1016/j.dsr.2008.05.014

———, L. Stemmann, L. Legendre, M. Picheral, L. Prieur, and G. Gorsky. 2007. Vertical distribution of aggregates (>110 μm) and mesoscale activity in the northeastern Atlantic: Effects on the deep vertical export of surface carbon. Limnol. Oceanogr. **52:** 7–18.

Hansen, J., T. Kiørboe, and A. Alldredge. 1996. Marine snow derived from abandoned larvacean houses: Sinking rates, particle content and mechanisms of aggregate formation. MEPS **141:** 205–215, doi:10.3354/meps141205

Honjo, S. 1996. Fluxes of particles to the interior of the open oceans, p. 91–113. *In* V. Ittekkot, P. Schäfer, S. Honjo, and P. J. Depetris [eds.], Particle flux in the ocean. Wiley.

Iversen, M. H., N. Nowald, H. Ploug, G. A. Jackson, and G. Fischer. 2010. High resolution profiles of vertical particulate organic matter export off Cape Blanc, Mauritania: Degradation processes and ballasting effects. Deep-Sea Res. I **57:** 771–784, doi:10.1016/j.dsr.2010.03.007

Jackson, G. A., R. Maffione, D. K. Costello, A. L. Alldredge, B. E. Logan, and H. G. Dam. 1997. Particle size spectra between 1 μm and 1 cm at Monterey Bay determined using multiple instruments. Deep-Sea Res. I **45:** 1739–1767, doi:10.1016/S0967-0637(97)00029-0

———, A. M. Waite, and P. W. Boyd. 2005. Role of algal aggregation in vertical carbon export during SOIREE and in other low biomass environments. Geophys. Res. Lett. **32:** L13607, doi:10.1029/2005GL023180

Komar, P. 1980. Settling velocities of circular cylinders at low Reynolds numbers. J. Geol. **88:** 327–336, doi:10.1086/628510

Lamborg, C., and others. 2008. The flux of bio-and lithogenic material associated with sinking particles in the mesopelagic twilight zone of the northwest and North Central Pacific Ocean. Deep-Sea Res. II **55:** 1540–1563, doi:10.1016/j.dsr2.2008.04.011

Lee, C., and others. 2009. Particulate organic matter and ballast fluxes measured using time-series and settling velocity sediment traps in the northwestern Mediterranean Sea. Deep-Sea Res. II **56:** 1420–1436, doi:10.1016/j.dsr2.2008.11.029

Lundsgaard, C. 1995. Use of a high viscosity medium in studies of aggregates, p. 141–152. *In* S. Floderus, A. S. Heisakanen, M. Oleson, and P. Wassman [eds.], Sediment trap studies in the Nordic countries. 3. Proceedings of the Symposium on Seasonal Dynamics of Planktonic Ecosystems and Sedimentation in Coastal Nordic Waters. Finnish Environment Agency.

Passow, U., R. F. Shipe, A. Murray, D. K. Pak, M. A. Brzezinski, and A. L. Alldredge. 2001. The origin of transparent exopolymer particles (TEP) and their role in the sedimentation of particulate matter. Cont. Shelf Res. **21:** 327–346, doi:10.1016/S0278-4343(00)00101-1

Peterson, M. L., S. G. Wakeham, C. Lee, M. A. Askea, and J. C. Miquel. 2005. Novel techniques for collection of sinking particles in the ocean and determining their settling rates. Limnol. Oceanogr.: Methods **3:** 520–532.

Ploug, H., M. H. Iversen, and G. Fischer. 2008. Ballast, sinking velocity, and apparent diffusivity within marine snow and zooplankton fecal pellets: Implications for substrate turnover by attached bacteria. Limnol. Oceanogr. **53:** 1878–1886.

Sarmiento, J. L., and N. Gruber. 2006. Ocean biogeochemical dynamics. Princeton Univ. Press.

Shanks, A. L., and J. D. Trent. 1980. Marine snow: Sinking rates and potential role in vertical flux. Deep-Sea Res. **27:** 137–143.

Sicko-Goad, L., C. Schelske, and E. Stoermer. 1984. Estimation of intracellular carbon and silica content of diatoms from natural assemblages using morphometric techniques. Limnol. Oceanogr. **29:** 1170–1178, doi:10.4319/lo.1984.29.6.1170

Silver, M. W., and A. L. Alldredge. 1981. Bathypelagic marine snow: Deep-sea algal and detrital community. J. Mar. Res. **39:** 501–530.

Stemmann, L., G. A. Jackson, and D. Ianson. 2004. A vertical model of particle size distributions and fluxes in the midwater column that includes biological and physical processes—part I: Model formulation. Deep-Sea Res. I **51:** 865–884, doi:10.1016/j.dsr.2004.03.001

Trull, T., S. G. Bray, K. O. Buesseler, C. H. Lamborg, S. Manganini, C. Moy, and J. Valdes. 2008. In situ measurement of mesopelagic particle sinking rates and the control of carbon transfer to the ocean interior during the Vertical Flux in the Global Ocean (VERTIGO) voyages in the North Pacific. Deep-Sea Res. II **55:** 1684–1695, doi:10.1016/j.dsr2.2008.04.021

Turner, J. T. 2002. Zooplankton fecal pellets, marine snow and sinking phytoplankton blooms. Aquat. Microb. Ecol. **27:** 57–102, doi:10.3354/ame027057

Volk, T., and M. I. Hoffert. 1985. Ocean carbon pumps—analysis of relative strengths and efficiencies in ocean-driven atmospheric CO2 changes, p. 99–110. *In* The carbon cycle and atmospheric CO2: Natural variations archean to present. Geophysical Monograph 32. American Geophysical Union.

Waite, A., and S. Nodder. 2001. The effect of in situ iron addition on the sinking rates and export flux of Southern Ocean diatoms. Deep-Sea Res. II **48:** 2635–2654, doi:10.1016/S0967-0645(01)00012-1

Walsh, I. D., and W. D. Gardner. 1992. A comparison of aggregate profiles with sediment trap fluxes. Deep-Sea Res. **39:** 1817–1834.

Xue, J., and R. A. Armstrong. 2009. An improved "benchmark" method for estimating particle settling velocities from time-series sediment trap fluxes. Deep-Sea Res. II **56:** 1479–1486, doi:10.1016/j.dsr2.2008.11.033

Associate editor: Thomas Kiørboe

Received: 16 March 2010
Accepted: 21 June 2010
Amended: 07 July 2010